MICROSTRIP REALIZATION OF TRISECTION SYNTHESIS WITH FREQUENCY-DEPENDENT ADMITTANCE INVERTER

C.-L. Hsu

Department of Computer and Communication Engineering
Ta Hwa Institute of Technology
Qionglin, Hsinchu 307, Taiwan

J.-T. Kuo

Department of Electronic Engineering
Chang Gung University, Taoyuan, Taiwan

Abstract—Frequency-dependent admittance (J-) inverter is incorporated in synthesis of microstrip trisection filters to achieve a quasi-elliptic function response. In the admittance matrix of the lowpass prototype, certain coupling is modeled by a constant J-inverter multiplied by the complex frequency variable s. Direct synthesis of three lowpass prototypes is presented. Based on the standard lowpass to bandpass transformation, coupled microstrip resonators with both electric and magnetic coupling are devised to implement the J-inverter with desired frequency-dependent characteristics. Tapped-line input/output is used and several transmission zeros can be created in the upper and lower rejection bands. In experiments, a third-order filter with four zeros, a fourth-order circuit with three zeros, and a fourth-order filter with five zeros are designed and fabricated. Measured results are compared with the simulation responses to validate the theory.

1. INTRODUCTION

Bandpass filters with a quasi-elliptic function response are very attractive in implementing the RF front-ends of wireless communication systems since excellent frequency selectivity can be obtained with a low circuit order. The selectivity is achieved by the two transmission

zeros on both sides of the passband. For microstrip realization, reduction of number of resonators is particularly important. This is because not only the circuit area can be saved but also insertion loss can be improved since such resonators usually have a relatively low quality (Q) factor.

It is well-known that the conventional 2×2 configuration, i.e., a quadruplet [1–3], possesses a pair of transmission zeros on both sides of the passband due to the cross coupling between the first and the last resonator. Many microstrip filters with a quasi-elliptic function passband have been realized. The realized circuits in [4] achieve a rejection of $50\,\mathrm{dB}$ at the two zero frequencies, in addition to a wide upper stopband. The multimode resonators in [5, 6] are also suitable for creating such passbands. The design in [7] with miniaturized spiral-shaped resonators with rectangle window feed structure also realizes transmission zeros on both sides of the passband.

Obviously, a rigorous synthesis procedure, e.g., [8], is required for creation of such zeros. In [9], a particular coupling scheme is arranged for source, load and a triple-mode cavity to realize a third-order filter with a pair of zeros. In [10], fourth-order canonical filters with source-load cross-coupling are developed to generate four zeros. Theoretically, for a coupled-resonator filter of order N with frequency-independent coupling, the maximal number of finite transmission zeros is N. If frequency-dependent coupling is used, however, a third-order filter may have four zeros [11]. In [12], a box-like coupling scheme including a two-mode resonator accompanied by a hairpin resonator is proposed to realize a third-order filter with a pair of zeros. Increasing number of zeros around the passband can greatly enhance the frequency selectivity so that the number of resonating elements can be reduced. This is accompanied with several advantages including low insertion loss in the passband, easy design and a compact circuit size.

In this paper, Section 2 describes synthesis of third- and fourth-order filters with a quasi-elliptic function response. A trisection configuration with a frequency-dependent admittance or J-inverter is proposed to generate the zeros. The configuration has at least three attractive properties. First, the condition of the zeros is very simple and involves only two circuit elements in the lowpass prototype. Second, in the admittance matrix of the lowpass prototype, all diagonal elements are not required to add any reactive elements. Third, when a higher order circuit is designed, the trisection can be cascaded with other resonators by direct coupling. Section 3 describes synthesis of three lowpass prototypes. The element values are analytically derived by matching the two-port $ABCD$ matrix entries with those derived from the prescribed insertion loss functions. Section 4 describes the

microstrip realization of the frequency-dependent J-inverters, Section 5 compares measured responses of experimental circuits with theoretical prediction and simulation, and Section 6 draws the conclusion.

2. SYNTHESIS AND CONDITION OF FINITE ZERO

When a two-port network has N_z finite transmission zeros and unity source and load impedance, its $ABCD$ matrix can be written as [13]

$$[ABCD] = \frac{1}{P(s)/\varepsilon} \left[\begin{array}{cc} A(s) & B(s) \\ C(s) & D(s) \end{array} \right] \tag{1a}$$

$$P(s) = \prod_{n=1}^{N_z} \left(1 - \frac{s}{s_{zn}} \right) \tag{1b}$$

where N_z is less than the circuit order N, s_{zn} denotes the nth zero and the constant ε specifies the inband ripple level. The polynomials in (1a) can be derived from the insertion loss function with a general Chebyshev form [13]

$$C_N = \cosh \left[\sum_{n=1}^{N} \cosh^{-1}(x_n(\Omega)) \right] \tag{2a}$$

$$x_n(\Omega) = \frac{\Omega - 1/\Omega_n}{1 - \Omega/\Omega_n} \tag{2b}$$

where $\Omega = s/j$ and $\Omega_n = s_{zn}/j$, where s is the complex frequency variable. Fig. 1 plots the responses of a third-order and a fourth-order Chebyshev filter with a 0.1-dB inband ripple level to be realized in this paper. The former and the latter circuits are designated to have
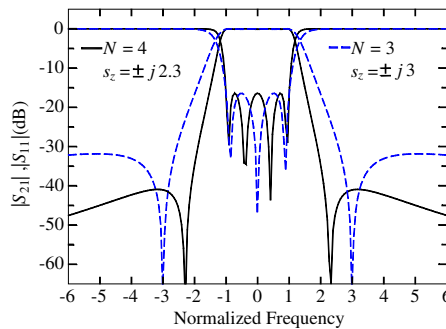
Figure 1. Lowpass Chebyshev responses of the third- and fourth-order prototype filters to be synthesized. Passband ripple = 0.1 dB.

zeros at $\pm j3$ and $\pm j2.3$, and the corresponding rejection levels in the stopband are 31 and 40 dB, respectively. Based on (1), (2) and the procedure described in [13], it can be derived that for the third-order filter,

$$A(s) = D(s) = 1.0949s^2 + 1 \tag{3a}$$
$$B(s) = 1.0298s \tag{3b}$$
$$C(s) = 1.1521s^3 + 1.9106s \tag{3c}$$

and for the fourth-order filter,

$$A(s) = D(s) = 1.9633s^3 + 2.2588s \tag{4a}$$
$$B(s) = 2.2051s^4 + 4.0108s^2 + 1.1642 \tag{4b}$$
$$C(s) = 1.7482s^2 + 0.85896 \tag{4c}$$

The coefficients of the polynomials in (3) and (4) are used to determine the element values of lowpass prototypes as follows. Fig. 2 shows two circuits capable of generating a pair of transmission zeros using a frequency-dependent J-inverter represented by sJ. The circuit in Fig. 2(a) has two signal paths from the input to the output port. One is the frequency-dependent J-inverter and the other is a cascade of two unity J-inverters with a shunt capacitor $C = sg$ in between. The Y-matrix of the upper path is

$$[Y] = sJ \begin{bmatrix} 0 & 1 \\ 1 & 0 \end{bmatrix} \tag{5}$$

where a phase shift of 90° is assumed [14], and that of the lower path can be derived as

$$[Y] = \frac{1}{sg} \begin{bmatrix} 1 & 1 \\ 1 & 1 \end{bmatrix} \tag{6}$$

The transmission zeros can be obtained by enforcing Y_{21} of the entire network to zero, i.e.,

$$s^2 = -\frac{1}{Jg} \tag{7}$$

The two zeros $s = \pm j\Omega_z = \pm j/\sqrt{Jg}$ if $Jg > 0$ holds, and they are purely imaginary and symmetric about the real axis in the complex frequency plane.

For the network in Fig. 2(b), one can treat the whole circuit as a four-port, derive its Y-matrix, reduce the four-port to a two-port by setting ports 2 and 3 open circuit, and then enforce Y_{41} of the resultant two-port to zero. It leads to

$$s^2 = -\frac{1}{2gJ - J^2} \tag{8}$$
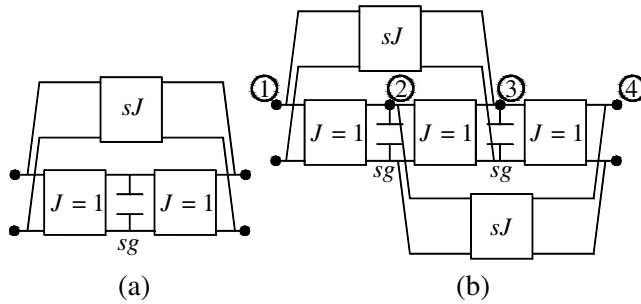
Figure 2. wo circuits with frequency-dependent J-inverters for generating a pair of transmission zeros. (a) A single trisection. (b) Two trisections.

For a prescribed transmission zero Ω_z, the J-inverter value is only about one half of that in (7). It will be shown later that number of design parameters of the fourth-order filter is less than that of a filter of the same order constructed by cascading the trisection in Fig. 2(a) with an additional resonator.

3. CIRCUIT SYNTHESIS

Figure 3 plots three possible lowpass prototypes built with the trisections in Fig. 2. Fig. 3(a) is a third-order circuit, and Fig. 3(b) and Fig. 3(c) are fourth-order circuits with one and a cascade of two trisections, respectively. The element values of these circuits will be determined by matching the coefficients of their $ABCD$ polynomials with those in (3) and (4). The $ABCD$ matrix of the two-port in the dashed-line box in Fig. 3(a) can be derived as

$$\begin{bmatrix} A & B \\ C & D \end{bmatrix} = \frac{1}{1 + s^2 Jg} \begin{bmatrix} -1 & -sg \\ sJ\left(2 + s^2 Jg\right) & -1 \end{bmatrix} \tag{9}$$
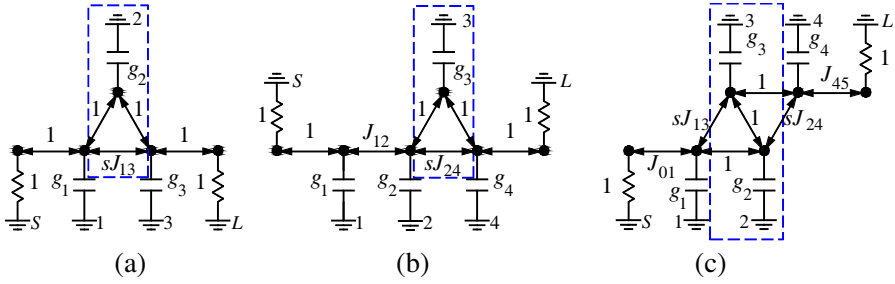
Thus, for the whole circuit

$$A(s) = D(s) = g_2 g_3 s^2 + 1 \tag{10a}$$

$$B(s) = g_2 s \tag{10b}$$

$$C(s) = \left(g_1 g_2 g_3 - \frac{J_{13}^2}{g_2}\right) s^3 + (g_1 + g_3 - 2J_{13}) s \tag{10c}$$

By letting $g_1 = g_3$ and matching the coefficients in (10) with those in (3), we obtain $g_1 = 1.0632$, $g_2 = 1.0298$, and $J_{13} = 0.1079$. Hence the

Figure 3. Three lowpass circuit prototypes. (a) Third-order circuit. (b) Fourth-order circuits with a cascade of an additional resonator and one trisection. (c) Fourth-order circuits with a cascade of two trisections.

admittance matrix can be written as

$$[Y] = \begin{bmatrix} 1 & j & 0 & 0 & 0 \\ j & s1.0632 & j & s0.1079 & 0 \\ 0 & j & s1.0298 & j & 0 \\ 0 & s0.1079 & j & s1.0632 & j \\ 0 & 0 & 0 & j & 1 \end{bmatrix} \tag{11}$$

where the $(1,1)$th and $(5,5)$th elements denote the source and load resistors, respectively.

For the fourth-order prototypes in Fig. 3(b), an extra resonator is cascaded with the trisection and the full $ABCD$ matrix can be derived as

$$A(s) = D(s) = \frac{g_1 g_2 g_3}{J_{12}} s^3 + \frac{g_1 + g_3 J_{12}^2}{J_{12}} s \tag{12a}$$

$$B(s) = \frac{g_1 g_2 g_3 g_4 - g_1 g_3 J_{24}^2}{J_{12}} s^4 + \left(\frac{g_1 (g_2 + g_4 - 2J_{24})}{J_{12}} + J_{12} g_3 g_4 \right) s^2 + J_{12} \tag{12b}$$

$$C(s) = \frac{g_2 g_3}{J_{12}} s^2 + \frac{1}{J_{12}} \tag{12c}$$

By matching the coefficients with those in (4), its admittance matrix can be written as

$$[Y] = \begin{bmatrix} 1 & j & 0 & 0 & 0 & 0 \\ j & s1.1232 & j1.1642 & 0 & 0 & 0 \\ 0 & j1.1642 & s1.8309 & j & s0.1701 & 0 \\ 0 & 0 & j & s1.1115 & j & 0 \\ 0 & 0 & s0.1701 & j & s1.1390 & j \\ 0 & 0 & 0 & 0 & j & 1 \end{bmatrix} \tag{13}$$

It is found that J_{12} ($= 1.1642$) is not a unity inverter and that $g_1 \neq g_4$, $g_2 \neq g_3$ and $J_{13} \neq J_{24}$, since the circuit is not symmetric. The circuit symmetry can be restored if two trisections are properly arranged as shown in Fig. 3(c). The $ABCD$ matrix for the circuit in the dashed-line box involves polynomials of degrees greater than two. The degrees, however, can be reduced by using the approximation $|J| \ll 1$. It leads to

$$\begin{bmatrix} A & B \\ C & D \end{bmatrix} = \frac{j}{1 + s^2 \left(2Jg - J^2\right)} \begin{bmatrix} s(g - 2J) & 1 \\ s^2 g^2 + 1 & s(g - 2J) \end{bmatrix} \quad (14)$$

This matrix is not strictly reciprocal since $AD - BC \neq 1$ due to the approximation. Nevertheless, the deviation is so small that the approximation is still accurate enough for the following synthesis. Let $g_1 = g_4$, $g_2 = g_3$, $J_{01} = J_{45}$, and $J_{13} = J_{24}$, the total $ABCD$ matrix becomes

$$A(s) = D(s) = g_1 g_2^2 s^3 + (g_1 + g_2 - -2J_{13})s \quad (15a)$$
$$B(s) = \left[g_1^2 g_2^2 s^4 + g_1(g_1 + 2g_2 - -4J_{13})s^2 + 1\right] / J_{01}^2 \quad (15b)$$
$$C(s) = \left(g_2^2 s^2 + 1\right) J_{01}^2 \quad (15c)$$

Because of symmetry, the circuit in Fig. 3(c) has two synthesis parameters less than the asymmetric structure in Fig. 3(b). One is that the external Q of the input and output resonators can be realized by the same coupling structure and the other is that only two, instead of three in Fig. 3(b), adjacent coupling coefficients have to be realized. The admittance matrix of the entire network can be written as

$$[Y] = \begin{bmatrix} 1 & j0.9268 & 0 & 0 & 0 & 0 \\ j0.9268 & s0.9647 & j & s0.06787 & 0 & 0 \\ 0 & j & s1.4266 & j & s0.06787 & 0 \\ 0 & s0.06787 & j & s1.4266 & j & 0 \\ 0 & 0 & s0.06787 & j & s0.9647 & j0.9268 \\ 0 & 0 & 0 & 0 & j0.9268 & 1 \end{bmatrix} \quad (16)$$

Since our aim is to design a high-selectivity filter with a small number of resonators, only synthesis of networks of order $N \leq 4$ is considered. However, high-order filters with more transmission zeros can be constructed by cascading the trisections, like that shown in Fig. 3(c).

In circuit realization, the frequency-independent coupling coefficients between adjacent resonators can be obtained from the matrices in (11), (13), and (16) and expressed as [14, 15]

$$K_{j,j+1} = \Delta \frac{J_{j,j+1}}{\sqrt{g_j g_{j+1}}} \quad (17a)$$

where Δ is the fractional bandwidth. Through a weak coupling test, the simulation $|S_{21}|$ of two coupled resonators will present two peaks. If the peak frequencies are f_a and f_b, the coupling coefficient can be calculated as

$$K_{j,j+1} = \frac{f_b^2 - f_a^2}{f_b^2 + f_a^2} \tag{17b}$$

Design graphs for coupling coefficient versus gap size can then be obtained. The external Q (Q_{ext}) of an Nth-order circuit is related to the bandwidth by [14]:

$$(Q_{ext})_i = \frac{g_0 g_1}{\Delta J_{01}^2} \tag{18a}$$

$$(Q_{ext})_o = \frac{g_N g_{N+1}}{\Delta J_{N,N+1}^2} \tag{18b}$$

where g_0 and g_{N+1} represent the source and load resistances, respectively. The position of the input and output ports is determined by matching singly loaded Q (Q_{si}) of the tapped resonator with external Q (Q_{ext}) of the filter in (18).

4. MICROSTRIP REALIZATION OF FREQUENCY-DEPENDENT J-INVERTER

In the lowpass prototypes in Fig. 3, the frequency-dependent J-inverter has a form of sJ. From the standard lowpass to bandpass transformation, i.e., $s \rightarrow j(\omega/\omega_0 - \omega_0/\omega)/\Delta$, the coupling coefficient between resonators j and $j + 2$, i.e., sJ_{13} and sJ_{24}, can be written as
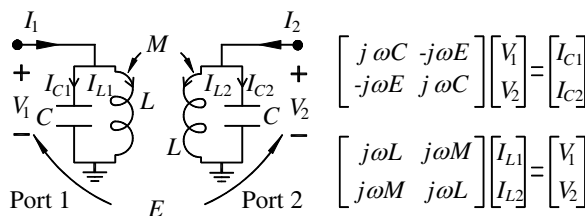
$$K_{j,j+2}\left(\frac{\omega}{\omega_0} - \frac{\omega_0}{\omega}\right) = \frac{J_{j,j+2}}{\sqrt{g_j g_{j+2}}}\left(\frac{\omega}{\omega_0} - \frac{\omega_0}{\omega}\right) \tag{19}$$

where ω_0 is the center frequency and Δ the fractional bandwidth. The J-inverter can be implemented by the coupling between two coupled resonators as modeled by the parallel-LC network in Fig. 4 [16], where both magnetic and electric coupling exist between the inductors and capacitors. From the equations in Fig. 4, the two-port Y-parameters can be derived as

$$Y_{21} = -j\sqrt{\frac{C}{L_r}}\left(\frac{E}{C}\frac{\omega}{\omega_0} - \frac{M}{L}\frac{\omega_0}{\omega}\right) \tag{20a}$$

$$Y_{11} = j\sqrt{\frac{C}{L_r}}\left(\frac{\omega}{\omega_0} - \frac{\omega_0}{\omega}\right) \tag{20b}$$

Figure 4. Lumped-circuit model for the frequency-dependent J-inverter between two coupled resonators.

where $\omega_0 = 1/\sqrt{L_r C}$ and $L_r = L(1 - M^2/L^2)$. Comparison of (19) and (20a) reveals that the frequency-dependent J-inverter can be realized if $E/C = M/L$ and

$$K_{j,j+2} = \frac{J_{j,j+2}}{\sqrt{g_j g_{j+2}}} = -\frac{E}{C} \qquad (21)$$

Based on (20a) and (20b), E/C can be obtained by simply calculating $-Y_{21}/Y_{11}$. However, both $Y_{21} = 0$ and $Y_{11} = 0$ at $\omega = \omega_0$. In this case, the L'Hospital rule can be used to extract the E/C from simulation or measurement Y_{21} and Y_{11} data. Let $b_{21} = \text{Im}[Y_{21}]/Y_0$ and $b_{11} = \text{Im}[Y_{11}]/Y_0$, then $K_{j,j+2}$ can be formulated as

$$K_{j,j+2} = -\left(\frac{db_{21}}{d\omega} \bigg/ \frac{db_{11}}{d\omega} \right)\bigg|_{\omega = \omega_0} \qquad (22)$$

where $Y_0 = 1/Z_0$ and Z_0 is port impedance. In case of $b_{11} \neq b_{22}$, (22) should be modified to

$$K_{j,j+2} = -\left(\frac{db_{21}}{d\omega} \bigg/ \sqrt{\left| \frac{db_{11}}{d\omega} \times \frac{db_{22}}{d\omega} \right|} \right)\bigg|_{\omega = \omega_0} \qquad (23)$$

Note that this frequency-dependent J-inverter is not adequate for coupling between adjacent resonators on the main signal path since $E/C = M/L$ holds and the net coupling is zero at $\omega = \omega_0$. It will be useful, however, for non-adjacent coupling to create finite transmission zeros near ω_0. Such frequency-dependent electric/magnetic coupling has been revealed among the combline resonators in [17], where these two types of coupling, however, are intentionally suppressed in order to obtain frequency-independent coupling since in circuit synthesis each off-diagonal element in the coupling matrix is assumed constant.

The microstrip structures in Fig. 5 are devised to realize the frequency-dependent J-inverters, which are used for experimental filters in the later sections. The electric coupling (E/C) mainly relies
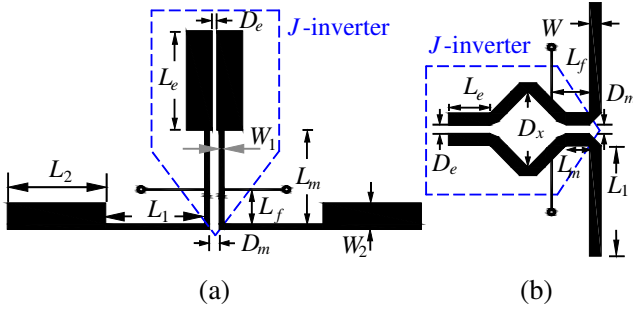
Figure 5. Microstrip frequency-dependent J-inverters. (a) Coupled stepped-impedance resonators. Sizes in mm: $D_m = 0.79$, $L_1 = 7.79$, $L_2 = L_e = 7.59$, $L_m = 7.19$, $L_f = 1.95$, $W_1 = 0.4$, $W_2 = 2$. (b) Coupled sections. Sizes in mm: $D_e = 0.3$, $D_m = 0.38$, $D_x = 8.94$, $L_1 = 21.36$, $L_e = 5.38$, $L_f = 3.35$, $L_m = 3.03$, $W = 1.55$. Substrate: $\varepsilon_r = 2.2$, thickness $= 0.508$ mm.
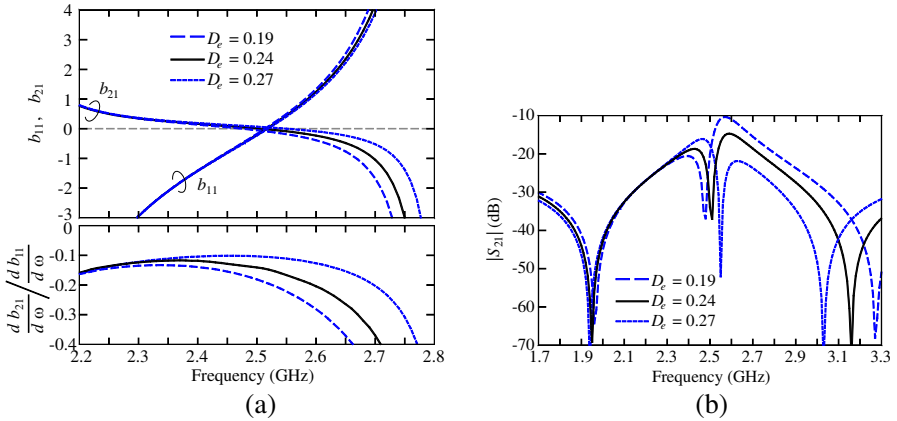
Figure 6. (a) Normalized susceptances and (b) $|S_{21}|$ responses of the J-inverter in Fig. 5(a).

on the open ends of the coupled resonators while the magnetic coupling (M/L) on the middle section. The sizes L_e, L_m, D_e and D_m can be determined by fitting the b_{21} and b_{11} curves of the test circuit to those in (20). Fig. 6(a) plots simulation results of b_{21}, b_{11} and $(db_{21}/d\omega)(db_{11}/d\omega)$ for the circuit in Fig. 5(a) for $D_e = 0.19$, 0.23, and 0.27 mm using the simulation software package IE3D [18]. The circuit has a relative dielectric constant $\varepsilon_r = 2.2$, thickness $= 0.508$ mm, and port impedance $Z_0 = 50\,\Omega$. For the third-order circuit described

in (11), $K_{13} = 0.1079/\sqrt{g_1 g_3} = 0.1015$, and it can be realized by using $D_e = 0.27$ mm, from Fig. 6(a).

When D_e is decreased, Fig. 6(a) indicates that the magnitude of $(db_{21}/d\omega)/(db_{11}/d\omega)$ increases, especially at high frequencies. It implies that the upper zero will be more sensitive to the variation of D_e. Fig. 6(b) plots the $|S_{21}|$ response for the test circuit in Fig. 5(a). The $|S_{21}|$ responses have dips near 2.5 GHz since net coupling is zero. It is resulted from the cancelation of the electric and magnetic coupling. One can observe from the results in Fig. 6(b) that the upper zero created by the tapped-input/output is sensitive to the variation of D_e.

The coupling structure in Fig. 5(b) is close to the narrow-band hairpin-comb filters in [19] when the gap width $D_x = D_e$. The purpose of D_x is to add a degree of freedom to designing the microstrip J-inverters such that the cancelation of electric and magnetic coupling can occur at the resonant frequency as required by (19).
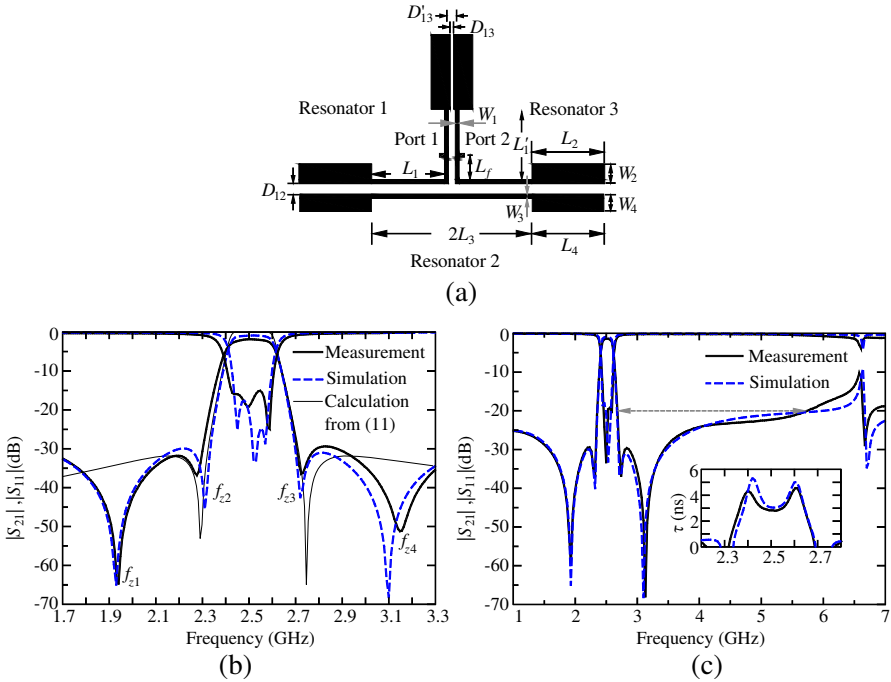
5. SIMULATION AND MEASUREMENT

All experimental circuits are designed at $f_0 = 2.5$ GHz and built on a substrate with $\varepsilon_r = 2.2$ and thickness $= 0.508$ mm. Fig. 7(a) shows the layout of the trisection filter based on the lowpass prototype in Fig. 3(a) with the admittance matrix in (11). The in-band ripple is 0.1 dB and $\Delta = 6\%$. The realization of the frequency-dependent J-inverter is in Fig. 5(a). The gap D_{12} is determined by the coupling coefficient $K_{12} = 0.0573$ from (17a). The tap point, denoted as L_f, is chosen to match the Q_{si} of the stepped-impedance resonator [20] to $Q_{ext} = 17.72$ in (18).

The lengths of the low-Z and high-Z sections of the first and third resonators in Fig. 7(a) are 7.59 and 7.79 mm, respectively. The 2.64% difference is resulted from fine-tuning of the final filter for recovering the resonance shift caused by the proximity effect of the second resonator. In our experience, the fine-tune process of the final filter parameters is inevitable; however, the parameters can rapidly converge when the initial values are properly given. The theoretical, simulated, and measured responses are shown in Fig. 7(b). There are four zeros in the stopband. The zeros f_{z1} and f_{z4} are created by the tapped-line while f_{z2} and f_{z3} are by the trisection. When the gap width D_{13} is too large to provide significant electric coupling, the J_{13}-inverter becomes magnetic coupling and purely frequency-independent, then only one zero in the lower stopband can be generated. In the passband, the measured insertion loss is 1.75 dB, and return loss is better than 15 dB. The rejection level in the upper stopband is -29.5 dB, which is merely 1.6 dB higher than the prediction. This deviation is due to

that the magnitude of $(db_{21}/d\omega)/(db_{11}/d\omega)$ increases when frequency is increased, as shown in lower part of Fig. 6(a). The broadband response in Fig. 7(c) shows that the measured 20 dB-rejection can be extended up to 5.75 GHz or $2.3f_0$. It is found that the peak at 6.57 GHz is caused by the first spurious resonance of resonator 2, of which the impedance ratio is slightly smaller that of the other resonators so that it has a lower first spurious resonance. The measured and simulated group delays (τ) are also given.

The second demonstration is a fourth-order filter based on the prototype in Fig. 3(b) with the admittance matrix in (13) using coupled uniform microstrip resonators. The J_{24}-inverter can be designed by a similar approach for the previous circuit except that one of the input/output feeds is replaced by a coupled-line. Then, (23) is used to calculate $K_{j,j+2}$ since $b_{11} \neq b_{22}$. The in-band ripple is 0.1 dB and

Figure 7. Layout, simulation and measured responses of the first circuit. (a) Layout. Dimensions in mm: $D_{12} = 0.47$, $D_{13} = 0.27$, $D'_{13} = 0.79$, $L_1 = 7.79$, $L'_1 = 7.19$, $L_2 = 7.59$, $L_3 = 8.58$, $L_4 = 7.42$, $L_f = 1.95$, $W_1 = W_3 = 0.4$, $W_2 = 2$, $W_4 = 1.74$. (b) $|S_{21}|$ and $|S_{11}|$ responses. (c) Group delay and broadband responses.

$\Delta = 5\%$. The circuit layout and responses are in Fig. 8. Note that one arm of resonator 2 is used to implement the J_{24}-inverter and the other is used to couple with resonators 1 and 3 by L_{12} and L_{23}, respectively. In Fig. 8(b), the zero f_{z1} is 0.4 GHz lower than prediction because the values of the J_{24}-inverter at low frequencies are slightly smaller than that it is specified by the $(3, 5)$th entry in (13). In measurement, the inband insertion loss is only 1.96 dB. It can be seen that the zero f_{z3} is determined by the tap point of port 1. If the alternative tap-point T', which has the same Q_{si} value, is used a zero will be produced in the lower stopband. This circuit has only three zeros; however, the frequency f_{z3} can be fully controlled by adjusting the length of L_{f1} with a proper line width of resonator 1 for matching the port impedance.

Figure 9(a) shows the circuit layout of a fourth-order filter based on the prototype in Fig. 3(c) with the admittance matrix in (16) with stepped-impedance resonators. Its in-band ripple and Δ are the same as those of the previous fourth-order circuit. Note that there are two identical frequency-dependent J-inverters, i.e., J_{13} and J_{24}, in the circuit. For establishing proper coupling between resonators 2 and 3, the two trisections are configured in a back-to-back arrangement with an offset distance S. Fig. 9(b) and Fig. 9(c) plot the simulation and measured responses. Five zeros around the passband can be observed. The upper rejection band is broadened by the zeros f_{z4} and f_{z5}. From the calculated response by (16) in Fig. 9(b), f_{z2} and f_{z3} are generated

(a)

(b)
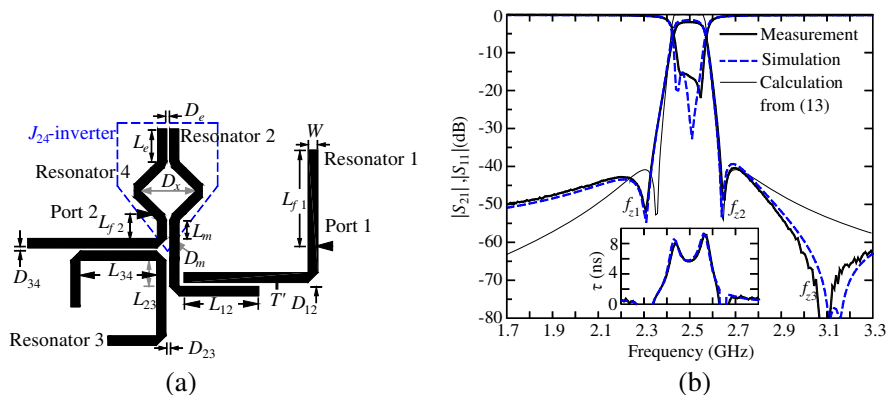
Figure 8. Layout, simulation and measured responses of the second circuit. (a) Circuit layout. Dimensions in mm: $D_{12} = 0.64$, $D_{23} = 0.46$, $D_{34} = 0.3$, $D_e = 0.3$, $D_m = 0.38$, $D_x = 8.94$, $L_{12} = 13.16$, $L_{23} = 4.61$, $L_{34} = 12.6$, $L_e = 5.38$, $L_{f1} = 17.12$, $L_{f2} = 3.35$, $L_m = 3.03$, $W = 1.55$. (b) Group delay, $|S_{21}|$ and $|S_{11}|$ responses.

by the trisection. Our circuit simulation indicates that the zeros f_{z1} and f_{z5} are dominated by the tapped-input/output structure. The position of the zero f_{z4} is affected by both; however, its generation mechanism is still unknown to the authors. The measured data show that the insertion loss is 2.34 dB at f_0, which is 0.38 dB higher than that of the second circuit due to the high-impedance segments. It is found that a rejection level of better than 40 dB can be achieved within the band covering from 2.64 to 4.91 GHz, and the stopband with a 30-dB rejection level is up to 6.03 GHz ($2.4 f_0$). The circuit size is $3.8 \times 3.3 \, \text{cm}^2$, about 55% of the area $5.8 \times 3.9 \, \text{cm}^2$ of the second circuit.
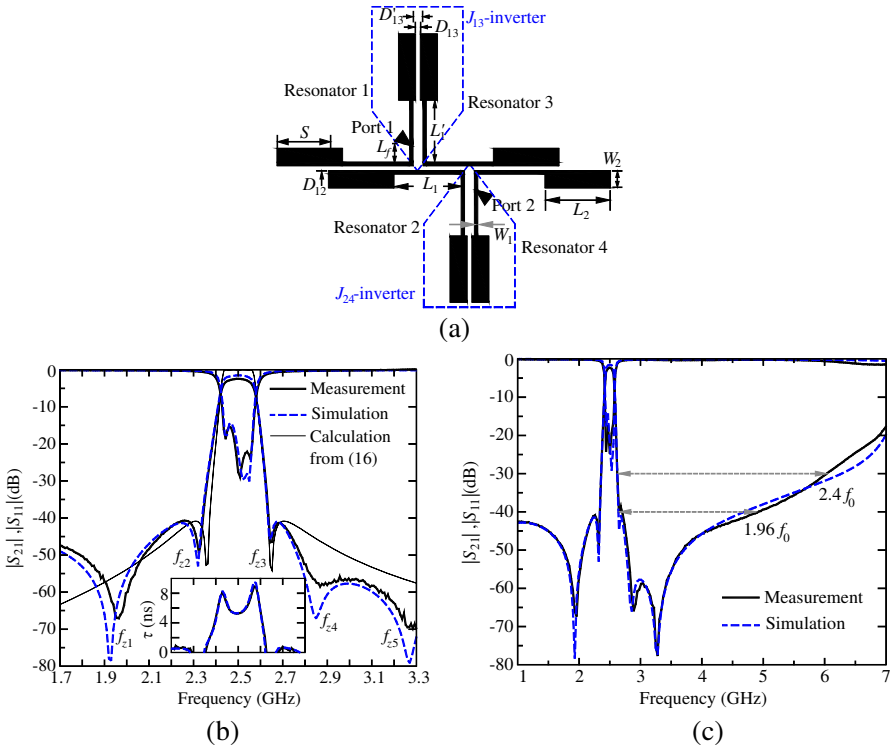
Figure 9. Layout, simulation and measured responses of the third circuit. (a) Circuit layout. Dimensions in mm: $D_{12} = 0.4$, $D_{13} = 0.19$, $D'_{13} = 0.79$, $L_1 = 7.79$, $L'_1 = 7.19$, $L_2 = 7.64$, $L_f = 1.95$, $S = 3.0$, $W_1 = 0.4$, $W_2 = 2$. (b) Group delay, $|S_{21}|$ and $|S_{11}|$ responses. (c) Broadband responses.

6. CONCLUSION

Coupled stepped-impedance resonators and uniform half-wave resonators are devised to implement the microstrip frequency-dependent J-inverters for synthesizing quasi-elliptic function passbands in trisection configuration. Direct synthesis of network elements has been developed for three lowpass prototypes by matching the coefficients of the two-port $ABCD$ polynomials. The elements in the synthesized admittance matrices have been used to determine the coupling coefficients and external Q values of the input/output resonators for the experimental filters. The synthesized third- and fourth-order filters present four and five transmission zeros, respectively. Simulation and theoretical prediction are validated by measured responses.

REFERENCES

1. Kurzrok, R. M., "General four-resonator filters at microwave frequencies," *IEEE Trans. Microw. Theory Tech.*, Vol. 14, 295–296, Jun. 1966.

2. Williams, E., "A four-cavity elliptic waveguide filter," *IEEE Trans. Microw. Theory Tech.*, Vol. 18, No. 12, 1109–1114, Dec. 1970.

3. Levy, R., "Direct synthesis of cascaded quadruplet (CQ) filters," *IEEE Trans. Microw. Theory Tech.*, Vol. 43, No. 12, 2940–2945, Dec. 1995.

4. Wu, H.-W., S.-K. Liu, M.-H. Weng, and C.-H. Hung, "Compact microstrip bandpass filter with multispurious suppression," *Progress In Electromagnetics Research*, Vol. 107, 21–30, 2010.

5. Zhang, L., Z.-Y. Yu, and S.-G. Mo, "Novel planar multimode bandpass filters with radial-line stubs," *Progress In Electromagnetics Research*, Vol. 101, 3342, 2010.

6. Mo, S.-G., Z.-Y. Yu, and L. Zhang, "Design of triple-mode bandpass filter using improved hexagonal loop resonator," *Progress In Electromagnetics Research*, Vol. 96, 117–125, 2009.

7. Dai, G.-L. and M.-Y. Xia, "Novel miniaturized bandpass filters using spiral-shaped resonators and window feed structures," *Progress In Electromagnetics Research*, Vol. 100, 235–243, 2010.

8. Wen, S. and L. Zhu, "Numerical synthesis design of coupled resonator filters," *Progress In Electromagnetics Research*, Vol. 92, 333–346, 2009.

9. Rosenberg, U. and W. Hagele, "Advanced multi-mode cavity filter design using source/load-resonance circuit cross couplings,"

IEEE Microw. Wireless Compon. Lett., Vol. 2, No. 12, 508–510, Dec. 1992.

10. Amari, S., "Direct synthesis of folded symmetric resonator filters with source-load coupling," *IEEE Microw. Wireless Compon. Lett.*, Vol. 11, No. 6, 264–266, Jun. 2001.

11. Amari, S. and J. Boremann, "Using frequency-dependent coupling to generate finite attenuation poles in direct-coupled resonator bandpass filters," *IEEE Microw. Wireless Compon. Lett.*, Vol. 9, No. 10, 404–406, Oct. 1999.

12. Liao, C.-K., P.-L. Chi, and C.-Y. Chang, "Microstrip realization of generalized Chebyshev filters with box-like coupling schemes," *IEEE Trans. Microwave Theory Tech.*, Vol. 55, No. 1, 147–153, Jan. 2007.

13. Cameron, R. J., C. M. Kudsia, and R. R. Mansour, *Microwave Filters for Communication Systems.*, Ch. 7, 245, Wiley, Hoboken, NJ, 2007.

14. Matthaei, G. L., L. Young, and E. M. T. Jones, *Microwave Filters, Impedance-matching Network, and Coupling Structures*, Ch. 4, 145 and Ch. 8, 433, Artech House, Norwood, MA, 1980.

15. Hong, J.-S. and M. J. Lancaster, "Couplings of microstrip square open-loop resonators for cross-coupled planar microwave filters," *IEEE Trans. Microw. Theory Tech.*, Vol. 44, No. 11, 2099–2109, Nov. 1996.

16. Kuo, J.-T., C.-L. Hsu, and E. Shih, "Compact planar quasi-elliptic function filter with in-line stepped-impedance resonators," *IEEE Trans. Microw. Theory Tech.*, Vol. 55, No. 8, 1747–1755, Aug. 2007.

17. Yao, H.-W., K.-A. Zaki, and A. E. Atia, "Full wave modeling of conducting posts in rectangular waveguides and its applications to slot coupled combline filters," *IEEE Trans. Microw. Theory Tech.*, Vol. 43, No. 12, 2824–2830, Dec. 1995.

18. IE3D simulator, Zeland Software Inc., Jan. 2002.

19. Matthaei, G. L., N. O. Fenzi, R. J. Forse, and S. M. Rohlfing, "Hairpin-comb filters for HTS and other narrow-band applications," *IEEE Trans. Microw. Theory Tech.*, Vol. 45, No. 8, 1226–1231, Aug. 1997.

20. Kuo, J.-T. and E. Shih, "Microstrip stepped-impedance resonator bandpass filter with an extended optimal rejection bandwidth," *IEEE Trans. Microw. Theory Tech.*, Vol. 51, No. 5, 1554–1559, May 2003.